Neurobiology of Aging 84 (2019) 17–25

Contents lists available at ScienceDirect

Neurobiology of Aging

journal homepage: www.elsevier.com/locate/neuaging

Microstructural changes in the brain mediate the association of AK4, IGFBP5, HSPB2, and ITPK1 with cognitive decline

Namhee Kim [a,b,*], Lei Yu [a,b], Robert Dawe [a,c], Vladislav A. Petyuk [d], Chris Gaiteri [a,b], Philip L. De Jager [e,f], Julie A. Schneider [a,b,g], Konstantinos Arfanakis [a,c,h], David A. Bennett [a,b]

[a] Rush Alzheimer's Disease Center, Rush University Medical Center, Chicago, IL, USA
[b] Department of Neurological Sciences, Rush University Medical Center, Chicago, IL, USA
[c] Department of Diagnostic Radiology and Nuclear Medicine, Rush University Medical Center, Chicago, IL, USA
[d] Biological Division, Pacific Northwest National Laboratory, Richland, WA, USA
[e] Center for Translational and Computational Neuroimmunology, Columbia University Medical Center, New York, NY, USA
[f] Cell Circuits Program, Broad Institute, Cambridge, MA, USA
[g] Department of Pathology, Rush University Medical Center, Chicago, IL, USA
[h] Department of Biomedical Engineering, Illinois Institute of Technology, Chicago, IL, USA

ARTICLE INFO

Article history:
Received 18 February 2019
Received in revised form 18 July 2019
Accepted 19 July 2019
Available online 26 July 2019

Keywords:
Postmortem brain
Transverse relaxation time
Brain protein
Brain pathology
Mediation analysis

ABSTRACT

The associations of 4 proteins—AK4, ITPK1, HSPB2, and IGFBP5—with cognitive function in older adults were largely unexplained by known brain pathologies. We examined the extent to which individual protein associations with cognitive decline were attributable to microstructural changes in the brain. This study included 521 participants (mean age 90.3, 65.9–108.3) with the postmortem reciprocal of transverse relaxation time (R_2) magnetic resonance image. All participants came from one of the 2 ongoing longitudinal cohorts of aging and dementia, the Religious Orders Study and Rush Memory and Aging Project. Higher abundance of AK4, HSPB2, and IGFBP5 was associated with faster cognitive decline and mediated through lower postmortem R_2 in the frontal and temporal white matter regions. In contrast, higher abundance of ITPK1 was associated with slower cognitive decline and mediated through higher postmortem R_2 in the frontal and temporal white matter regions. The associations of 4 proteins—AK4, ITPK1, IGFBP5, and HSPB2—with cognition in late life were explained via microstructural changes in the brain.

1. Introduction

RNA sequencing data from postmortem human brains showed a robust relationship between cognitive decline—a clinical hallmark of Alzheimer's dementia—and a network of coexpressed cortical genes (Mostafavi et al., 2018). This coexpressed network is likely related to transcriptional regulation and termed "module 109" (m109). The average expression of m109 was also related to burden of brain β-amyloid deposition—an Alzheimer's disease (AD) pathology (Mostafavi et al., 2018). In a subsequent study (Yu et al., 2018), we prioritized 30 genes of 390 genes involved in the m109 as potential drivers of the module. Of those 30 genes, 14 genes were tested for their knockdown of gene expression in human astrocyte cell culture derived from induced pluripotent stem cell and measured for its extracellular levels of the pathogenic β-amyloid $A\beta_{42}$ peptide. Of 14 genes, inositol polyphosphate phosphatase-like 1 (INPPL1) and plexin B1 (PLXNB1) RNA knockdown reproducibly reduced the production of pathogenic soluble $A\beta_{42}$. These experiments suggested that INPPL1 and PLXNB1 may play an important role of m109 on β-amyloid metabolism. Although m109 was causally implicated in Alzheimer's dementia in part through brain β-amyloid deposition, it also had a strong effect on cognitive decline that was independent of β-amyloid and age-related pathologies (Yu et al., 2018). Using selected reaction monitoring (SRM) quantitative proteomics, it was possible to quantify 12 of the corresponding proteins. We examined their association with AD and non-AD pathology beyond β-amyloid deposition, as well as cognitive decline. Of these, 5 proteins were associated with cognitive decline. The association of one protein—PLXNB1—with cognitive decline was mediated primarily through β-amyloid load and PHFtau tangle density. However, the associations of insulin-like growth factor binding protein 5

* Corresponding author at: 1750 W. Harrison St, Chicago, IL 60612, USA. Tel.: 312 563 9149; fax: 312 942 2297.
E-mail address: Namhee_Kim@rush.edu (N. Kim).

0197-4580/$ – see front matter © 2019 Elsevier Inc. All rights reserved.
https://doi.org/10.1016/j.neurobiolaging.2019.07.013

(IGFBP5) and heat shock protein family B member 2 (HSPB2) were only partially mediated by AD or other age-related pathologies—amyloid, PHFtau tangles, macroinfarcts, microinfarcts, Lewy bodies, hippocampal sclerosis, TDP stage 4, cerebral amyloid angiopathy (CAA), cerebral atherosclerosis, and arteriolosclerosis (Yu et al., 2018). Furthermore, adenylate kinase 4 (AK4) and inositol-tetrakisphosphate 1-kinase (ITPK1) were essentially independent of common brain pathologies (Yu et al., 2018). Interestingly, higher abundance of AK4, HSPB2, and IGFBP5 were associated with faster cognitive decline, whereas higher abundance of ITPK1 was associated with slower cognitive decline (Yu et al., 2018).

Recent combinations of molecular levels and neuroimaging have shown that many features of brain structure and function have analogues on the molecular level (Fulcher and Fornito, 2016; Krienen et al., 2016; Richiardi et al., 2015). These studies typically compare neuroimaging and molecular levels acquired from distinct areas of the brain. Because brains donated by participants from the Religious Orders Study (ROS) and Rush Memory and Aging Project (MAP) undergo postmortem imaging, it is possible to map the brain regions that covary with levels of a given molecule. To account for the unexplained covariation of AK4, HSPB2, IGFBP5, and ITPK1 with cognitive decline, we considered the potential for these proteins to play a role in maintaining or degrading microstructure. Therefore, we examined the extent to which brain microstructure as assessed with R_2 could mediate the association of these 4 brain proteins with cognitive decline. Among various postmortem brain imaging modalities, R_2, the reciprocal of transverse relaxation time (i.e., T_2) on MRI, has been studied for its association with late-life cognitive decline and brain pathologies (Arfanakis et al., 2007; Dawe et al., 2014a, 2016, 2018; House et al., 2006, 2008; Kirsch et al., 1992; Wang et al., 2004). For instance, previous reports have associated in vivo R_2 with different stages of memory impairment (House et al., 2006), where lower R_2 in widespread white matter regions and higher R_2 in the gray matter of the temporal lobe coincided with impaired memory. One potential cause of lower R_2, or higher T_2, in the white matter is increased water content in white matter tissue due to breakdown of myelin by neurodegenerative processes and vascular insults. Although biological mechanisms of neurodegeneration in the gray matter are more complicated (House et al., 2006), one cause for higher R_2 in the gray matter may be higher accumulation of iron. Higher iron content is known to cause local distortion of the magnetic field that leads to higher relaxation rate, i.e., shorter T_2 and thus higher R_2. Owing to the relevance of R_2 to both brain structure and cognition, we examine how it could mediate the relationship of protein abundance with cognition, particularly in cases when AD or other age-related pathologies do not account for their relationship. We utilize a subset of the same study subjects—ROS and MAP—that were the subject of prior work (Mostafavi et al., 2018; Yu et al., 2018) based on data metrics required for these analyses.

2. Methods

2.1. Participants

Participants were older adults enrolled in one of the two ongoing cohort studies of aging and dementia, ROS and MAP (Bennett et al., 2018). Both studies were approved by the Institutional Review Board of Rush University Medical Center, Chicago, IL, USA. As a condition of enrollment in ROS and MAP, participants agreed to annual assessments and brain donation after death. A written informed consent and an anatomical gift act were obtained from each participant. Participants entered the studies without known dementia. This study included autopsied participants with targeted SRM proteomics, neuropathologic data, and R_2 images from postmortem MRI that passed quality control. A total of 521 participants with both postmortem MRI and targeted SRM proteomics were used. Among those, 228 (43.8%) were clinically diagnosed with Alzheimer's dementia and 355 (68.1%) had pathologic AD. The average age at death was 90.3 years (standard deviation [SD]: 6.1; range 65.9–108.3). A majority were female (70.3%), and almost all were non-Latino whites (95.9%). The average years of education was 15.8 (SD: 3.6; range 3–30).

2.2. Cognitive assessment

A neuropsychological test battery was administered every year with over 95% overall follow-up rate. The cognitive battery consists of 21 tests, 19 in common between MAP and ROS, 17 of which were used to assess multiple domains of cognitive ability, including episodic, semantic, and working memory; perceptual speed; and visuospatial acuity. Each of the scores was z-transformed using baseline means and SDs, and the resulting z-scores from all tests were averaged to derive a composite measure of global cognition. We estimated person-specific rates of cognitive decline based on a linear mixed effects model adjusted for age, sex, and years of education, as previously reported (Yu et al., 2018).

2.3. Neuropathology measures

At autopsy, brains were removed and hemisected in accordance with standard protocol (Schneider et al., 2009). We identified the cerebral hemisphere with more visible pathology mainly based on gross infarcts, and occasionally tumor or hemorrhage. The hemisphere was immersed in 4% paraformaldehyde solution and refrigerated at 4 °C. The other hemisphere was frozen in preparation for use in various other investigations, including RNA proteomics. Neuropathologies, including AD, cerebral infarcts, Lewy bodies, hippocampal sclerosis, hyperphosphorylated transactive response DNA-binding protein 43 (TDP-43), CAA, atherosclerosis, and arteriolosclerosis were evaluated, blind to clinical diagnosis. β-amyloid and PHFtau tangle pathologies were measured using molecular-specific immunohistochemistry in 8 predetermined brain regions, including superior frontal cortex, dorsolateral prefrontal cortex (DLPFC), entorhinal cortex, and hippocampus, consisting of 20 μm sections immunostained with one of the three monoclonal antibodies (4G8, 1:9000; Covance Labs, Madison, WI, USA; 6F/3D, 1:50; Dako North America Inc, Carpinteria, CA, USA; and 10D5,1:600; Elan Pharmaceuticals, San Francisco, CA, USA) for β-amyloid and AT8 (1:1,000, Innogenetics, San Ramon, CA, USA) for PHFtau tangles (Bennett et al., 2006). β-amyloid load and PHFtau tangle density were obtained by image analysis utilizing Stereo Investigator, version 2017. For β-amyloid, positive regions of interest were manually outlined and analyzed at 20× using an Olympus BX51 microscope attached to an MBF CX9000 camera coupled to a stage driver. A grid was placed for sampling about 20%–25% area from neocortical regions and 40%–45% of the area from entorhinal and hippocampal sector CA1/subiculum cortices. The percent area of β-amyloid immunoreactivity (load) was then estimated using the Image J software and averaged across regions. For analyses, amyloid load was defined as the square root of the percent of tissue area that was positive for β-amyloid within each region averaged over all regions for each participant. PHFtau tangle neurons in each region was quantified after outlining the region of interest and using the optical fractionator probe and random sampling about 10%–15% area from the neocortex and 15% area from mesial temporal lobe

structures. Regional PHFtau tangle densities were averaged across regions. Macroscopic infarcts were recorded during gross examination and confirmed histologically, and microinfarcts were identified in a minimum of 9 regions per participant using hematoxylin and eosin (H&E) stain (Arvanitakis et al., 2011). Both chronic macroscopic infarcts and microinfarcts were recorded as presence/absence. Lewy bodies in the substantial nigra, limbic, and neocortical regions were identified using α-synuclein immunostaining (Schneider et al., 2012) and were recorded as present/absent. Hippocampal sclerosis was assessed using H&E-stained sections from the mid-hippocampus (Nag et al., 2015) and was recorded as presence/absence. We used monoclonal TDP-43 antibody (Yu et al., 2015b) to stain 6 regions (amygdala, CA1 of hippocampus, dentate of hippocampus, entorhinal cortex, and mid-temporal and mid-frontal cortices) and manually scanned slides at low power (4× objective) to find the greatest density of TDP-43 inclusions. Objective was then switched to 20 × objective, and counts were performed in a 0.25 mm^2 sampling frame (500 μm square). All TDP-43 inclusions were included, i.e., neuronal, neuronal intranuclear, and glial cytoplasmic. We used the presence or absence of TDP-43 across these 6 regions to stage the severity of progression of TDP-43 from stage 0 (no inclusions), to (1) amygdala only, to (2) extended to other limbic regions, to (3) extended to the neocortex. CAA pathology was assessed in 4 neocortical regions: mid-frontal, mid-temporal, angular, and calcarine cortices. Paraffin-embedded sections were immunostained for β-amyloid using 1 of 3 monoclonal anti-human antibodies: 4G8 (1:9000; Covance Labs), 6F/3D (1:50; Dako North America Inc), and 10D5 (1:600; Elan Pharmaceuticals). For CAA assessment, meningeal and parenchymal vessels were assessed for amyloid deposition and scored from 0 to 4, where 0 = no deposition, 1 = scattered segmental but no circumferential deposition, 2 = circumferential deposition up to 10 vessels, 3 = circumferential deposition up to 75% of the region, and 4 = circumferential deposition over 75% of the total region. The CAA score for each region was the maximum of the meningeal and parenchymal CAA scores. Scores were averaged across regions and summarized as a continuous measure of CAA pathology for analyses (Boyle et al., 2015, Yu et al., 2015a). Atherosclerosis was assessed by visual inspection of the segmental or circumferential subintimal accumulation of lipid, plasma proteins, and calcium deposition in the circle of Willis, of which the vertebral, basilar, posterior cerebral, middle cerebral, and anterior cerebral arteries and their proximal branches were inspected. Severity of atherosclerosis was graded based on the involvement of each artery and number of arteries from 0 (none) to 6 (severe) (Arvanitakis et al., 2017; Arvanitakis et al., 2016). On involvement of a new rater, we follow a standard protocol in which the new rater rates 50 to 100 slides that have already been rated by an experienced rater and must be certified on practice slides before actual data collection.

The slides are selected to include a representative range of pathology. We then obtain percent of variation in the square-root transformed value of amyloid and tangles due to raters within slide. Generally, the variance due to different raters is less than 5%. Similar cross-training is performed with TDP-43 data collection, and cerebrovascular and Lewy body disease pathologies are reviewed by a neuropathologist (Bennett et al., 2012).

2.4. Targeted SRM proteomics

Targeted proteomics analysis was performed using frozen tissue from 1226 DLPFC samples; the same brain region selected for RNAseq. Details on SRM methods are reported in our previous publications (Andreev et al., 2012; Kim et al., 2014; Petyuk et al., 2010; Yu et al., 2018). Peptide abundance is measured as a ratio of its intensity to the intensity of the spiked-in synthetic stable isotope-labeled standard. The endogenous light-to-labeled-heavy peptide ratios were log2-transformed and median-centered. This effectively made the log2 abundance ratios relative to the median abundance. The reproducibility and the quality of peptide quantification were assessed using repetitive measurements of pooled samples employed as technical controls. We considered a peptide signal informative if the variance, both technical and biological, across the individual brain samples exceeded 2-fold of technical variance. For proteins with multiple peptides quantified, the peptide with the highest signal-to-noise ratio (total/technical variance) was used.

2.5. MRI acquisition

At approximately 1-month postmortem (mean = 30 days; SD = 19.2 days), the refrigerated hemisphere at 4 °C from each decedent was imaged using a 3-Tesla MRI scanner after allowing the tissue to warm to room temperature. Four different scanners were used to acquire fast spin-echo T_2-weighted MRI data with at least 2 different echo times. Details of MRI acquisition have been previously reported (Dawe et al., 2009, 2014a, 2016, 2018). The transverse relaxation time constant, T_2, describing the decay rate of the transverse component of magnetization is sensitive to, among other things, brain tissue's free water content and the presence of paramagnetic materials, such as iron. As previously described (Dawe et al., 2014a, 2016, 2018), we quantified the reciprocal of T_2, R_2, to reduce skewness and achieve a more normally distributed signal. R_2 maps were spatially registered to a cerebral hemisphere template, using first linear and then nonlinear transformations (Dawe et al., 2016). To account for interscanner differences in R_2, we carried out a voxel-by-voxel normalization of R_2 values within each group of hemispheres imaged on a given scanner by subtracting the median and dividing by the interquartile range of R_2 for that scanner. In addition, we carried out spatial smoothing with full width at half maximum 2 mm. Details of postmortem MRI preprocessing procedure have been described previously (Dawe et al., 2014a, 2016, 2018).

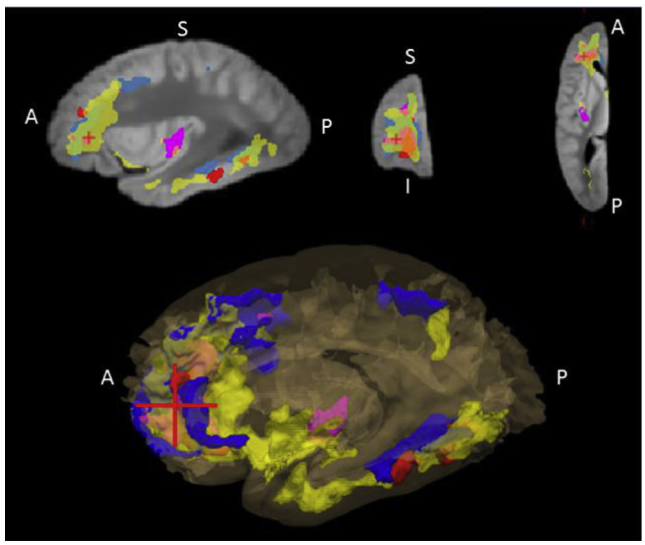

Fig. 1. Postmortem brain areas associated with each of the 4 proteins—AK4, ITPK1, IGFBP5, and HSPB2. A 3D view of all the clusters from the 4 proteins is shown in bottom panel, and its sagittal, coronal, and axial view at the red crosshair is shown in the top panel. The regions associated with AK4 are colored in pink, ITPK1 in blue, IGFBP5 in yellow, and HSPB2 in red. (For interpretation of the references to color in this figure legend, the reader is referred to the Web version of this article.)

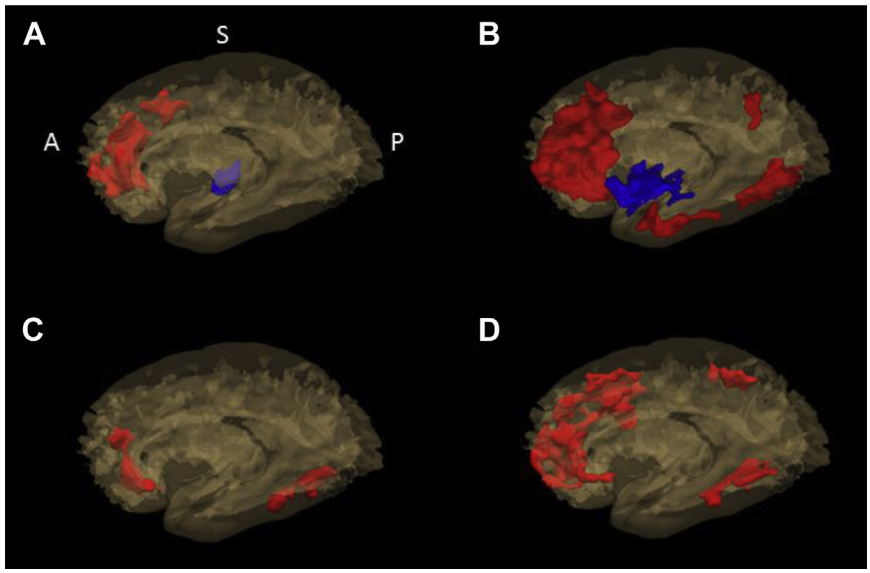

Fig. 2. Map of individual group of clusters associated with each of the 4 proteins—AK4, ITPK1, IGFBP5, and HSPB2. AK4 is shown in (A), IGFBP5 in (B), HSPB2 in (C), and ITPK1 in (D). Clusters grouped together were consistent in their major tissue types (white vs. gray). In each figure, the red-colored area shows the cluster group located in the white matter, and the blue-colored area in the gray matter. (For interpretation of the references to color in this figure legend, the reader is referred to the Web version of this article.)

2.6. Regions in the postmortem brain associated with individual proteins

Voxel-wise linear regression analysis was applied to each half-brain (number of voxels $\geq 4 \times 10^5$) to identify brain regions where postmortem R_2 was associated with abundance of each of our 4 proteins—AK4, ITPK1, IGFBP5, and HSPB2—after controlling for age at death, sex, and years of education. Thresholds were sequentially applied, first on individual voxels ($p < 0.01$) and then on individual clusters ($p < 0.05$ corrected for multiple comparisons) based on the random field theory (Friston et al., 1994; Worsley et al., 1996), a part of statistical parametric mapping. Principal component analysis (PCA), based on correlations of mean R_2 values between clusters, was used to reduce dimensionality (or number of clusters). For an instance, the first principal component (PC) is sufficient to explain total variation in R_2 clusters if all the clusters are highly mutually correlated. The number of PCs chosen was based on the proportion of variance explained. Assignment of individual clusters into groups was based on loadings of PCs. We illustrate this procedure with AK4 from Supplementary Material 1. The first two PCs explained 93% of the variance, whereas the 3rd PC only explained 7%. Therefore, the first two PCs were included in analyses. In PC_1, clusters 1 and 2 had almost equal loadings, whereas the loading of cluster 3 was one-tenth of those. Clusters 1 and 2 were therefore assigned to PC_1. The loading of cluster 3 suggested that it should be included in PC_2. Such disjoint sets are referred to as cluster groups. The mean value of postmortem R_2 from each cluster group was utilized for subsequent mediation analysis. It is noteworthy that our mediation analysis is a simplified approach with clusters while voxel-wise mediation approach is also available with intensive computation.

Table 1
Association of protein on cognitive decline after controlling demographic variables

Protein	Beta (total effect)	SE	*p*
AK4	−0.0173	0.0043	<0.0001
ITPK1	0.0147	0.0043	0.0006
IGFBP5	−0.0309	0.0041	<0.0001
HSPB2	−0.0138	0.0043	0.0013

Cognitive decline = demographic variables + protein.

2.7. Mediation analysis

We examined 3 models: (a) cognitive decline as a function of 3 demographic variables (age at death, sex, and years of education) and protein abundance; (b) postmortem R_2 as a function of the 3 demographic variables and protein abundance; and (c) cognitive decline as a function of the 3 demographic variables, protein abundance, and postmortem R_2. Because postmortem R_2 is known to be variably correlated with neuropathology, we repeated the analysis and included neuropathology measures in each step. In the mediation analysis, we tested the effect of each protein on cognitive decline through the aforementioned groups of R_2 clusters, also known as the *indirect effect*. The remaining effect of each protein on cognitive decline not acting through R_2 after controlling covariates—the *direct effect*—was calculated and the sum of these 2 effects constituted the total effect of each protein on cognitive decline, after controlling covariates. In the presence of multiple groups of R_2 clusters as mediators, we assessed individual indirect effects by individual mediators. Mediation analysis was performed by SAS macro provided by Hayes & Preacher (Hayes and Preacher, 2014).

3. Results

3.1. AK4, HSPB2, and IGFBP5 with a faster rate of cognitive decline

Voxel-wise postmortem R_2 analysis identified areas in the brain associated with abundance of each protein. Three clusters with a

Table 2
Association of protein on postmortem ex vivo R_2 after controlling demographic variables

Protein	Cluster group 1			Cluster group 2		
	Beta	SE	*p*	Beta	SE	*p*
AK4	−0.1520	0.0431	0.0004	0.170	0.0436	0.0001
ITPK1	0.2002	0.0425	<0.0001			
IGFBP5	−0.2099	0.0423	<0.0001	0.2509	0.0425	<0.0001
HSPB2	−0.1876	0.0421	<0.0001			

Postmortem R_2 = demographic variables + protein.
Cluster group 1 was mainly located in white matter while cluster group 2 was in gray matter.

Table 3
Association of protein on cognitive decline after controlling demographic variables and postmortem R_2

Protein		Protein			Cluster group 1			Cluster group 2		
		Beta	SE	*p*	Beta	SE	*p*	Beta	SE	*p*
AK4	Direct effect	−0.0088	0.0040	0.0301	0.0343	0.0040	<0.0001	−0.020	0.0040	<0.0001
Indirect effect	through C1	−0.0052	0.0017	0.0022						
Indirect effect	through C2	−0.0033	0.0013	0.0111						
ITPK1	Direct effect	0.0084	0.0041	0.0420	0.0315	0.0042	<0.0001			
Indirect effect	through C1	0.0063	0.0015	<0.0001						
IGFBP5	Direct effect	−0.0167	0.0039	<0.0001	0.0333	0.0039	<0.0001	−0.0287	0.0039	<0.0001
Indirect effect	through C1	−0.0070	0.0016	<0.0001						
Indirect effect	through C2	−0.0072	0.0015	<0.0001						
HSPB2	Direct effect	−0.0072	0.0041	0.0765	0.0348	0.0042	<0.0001			
Indirect effect	through C1	−0.0065	0.0016	<0.0001						

Cognitive decline = demographic variables + postmortem R_2 + protein.
Cluster group 1 was mainly located in the white matter, whereas cluster group 2 was in the gray matter.

total volume of 6563 (mm^3) in the postmortem brain template were identified for AK4, 6 clusters with a total volume of 29,535 (mm^3) for IGFBP5, and 2 clusters with a total volume of 4464 (mm^3) for HSPB2. As shown in Fig. 1, clusters were predominantly located in frontal, temporal, and parietal areas and exhibited a high degree of overlap. Based on the PCA results, the first PC for HSPB2, explaining 75.2% of the total variance, was chosen; For AK4 and IGFBP5, the first two PCs, explaining 92.9% and 73.0% of the total variance, were chosen, respectively. It is noteworthy that clusters grouped together were consistent in their major tissue types (white vs. gray matter). Of the 2 cluster groups, respectively, for AK4 and IGFBP5, cluster group 1 was mainly located in the white matter, and the cluster group 2 in the gray matter, whereas all the clusters from HSPB2 were in the white matter. By tissue types, lower R_2 cluster in the white matter and higher R_2 cluster in the gray matter was associated with more rapid cognitive decline. Individual groups of clusters are shown in Fig. 2A–C. In each panel, red-colored areas are for clusters mainly located in the white matter, and blue-colored areas are for clusters in the gray matter.

In mediation analysis, we examined the mediating role of the postmortem R_2 clusters on the relationship between each of the proteins and cognitive decline, adjusting for age, sex, and education. Higher AK4, HSPB2, and IGFBP5 were associated with faster decline in cognition (AK4: $\beta = -0.0173$, $p < 0.0001$; HSPB2: $\beta = -0.0138$, $p = 0.0013$; IGFBP5: $\beta = -0.0309$, $p < 0.0001$) (Table 1). The association between each protein and R_2 clusters is shown in Table 2. All 3 proteins showed significant indirect effects on cognitive decline through postmortem R_2 clusters (Table 3).

Because microstructural changes in the brain measured by postmortem R_2 is known to be correlated with various neuropathology measurements (Dawe et al., 2014a, 2016, 2018; House et al., 2008), we next examined the mediating role of microstructural changes in the brain measured by postmortem R_2 in the relationship between each of the 3 proteins (AK4, IGFBP5, and HSPB2) and cognitive decline, after adjusting for AD and other common neuropathologies, as well as age, sex, and education (Tables 4–6). Similar to the results of analyses not including neuropathology measures, the mediation effect of microstructural changes in the brain measured by postmortem R_2 on association between protein abundance and cognitive decline remained significant (Table 6). The proportion of indirect effects out of the total effect for each protein was about 50% (AK4 47%; IGFBP5 45%; HSPB2 50%) without adjusting neuropathology measures while it was about 40% (AK4 40%; IGFBP5 30%; HSPB2 43%) with neuropathology measures (Table 7). Diagrams for each mediation analysis are shown in Figs. 3–5.

Table 4
Association of protein on cognitive decline after controlling demographic variables and neuropathology

Protein	Beta (total effect)	SE	*p*
AK4	−0.0145	0.0035	<0.0001
ITPK1	0.0101	0.0035	0.0050
IGFBP5	−0.0203	0.0035	<0.0001
HSPB2	−0.0073	0.0036	0.0418

Cognitive decline = demographic variables + neuropathology + protein.

3.2. ITPK1 with a slower rate of cognitive decline

Voxel-wise postmortem R_2 analysis identified areas in the brain associated with ITPK1 abundance in 3 clusters, involving a total volume of 13,611 (mm^3). These clusters were all involved in the first PC with almost equal weights (accounting for 74.5% of the total variance) and mainly located in the white matter. Mediation effects of microstructural changes in the brain measured by postmortem R_2 on the relationship between ITPK1 and cognitive decline, adjusting for age, sex, and education, was tested. Higher ITPK1 abundance was associated with slower decline ($\beta = 0.0147$, $p = 0.0006$; Table 1). ITPK1 showed a significant indirect effect on cognitive decline through postmortem R_2 clusters ($\beta = 0.0084$, $p = 0.042$; Table 3). Proportion of indirect effect to the total effect of ITPK1 was 47% (Table 7). The mediation effect of postmortem R_2 clusters on the relationship between ITPK1 and cognitive decline, adjusting for AD and other common neuropathologies, in addition to age, sex, and education, is shown in Tables 4–6. Similar to our previous results, the mediation effect of postmortem R_2 clusters remained significant (Table 6). Diagram for each mediation analysis is shown in Fig. 6.

4. Discussion

We have previously reported that higher expression of the coexpressed gene set m109 results in greater β-amyloid pathology burden and more rapid cognitive decline, and these reports proposed 2 genes, INPPL1 and PLXNB1, as potential drivers of the network (Mostafavi et al., 2018). In a subsequent study, PLXNB1's involvement was further validated in 834 human autopsy samples

Table 5
Association of protein on postmortem ex vivo R_2 after controlling demographic variables and neuropathology

Protein	Cluster group 1			Cluster group 2		
	Beta	SE	*p*	Beta	SE	*p*
AK4	−0.1550	0.0407	0.0002	0.1660	0.0438	0.0002
ITPK1	0.1717	0.0406	<0.0001			
IGFBP5	−0.1584	0.0414	0.0001	0.1891	0.0427	<0.0001
HSPB2	−0.1622	0.0402	<0.0001			

Postmortem R_2 = demographic variables + neuropathology + protein.
Cluster group 1 was mainly located in the white matter, whereas cluster group 2 was in the gray matter.

Table 6
Association of protein on cognitive decline after controlling demographic variables, neuropathology, and postmortem R_2

Protein		Protein			Cluster group 1			Cluster group 2		
		Beta	SE	*p*	Beta	SE	*p*	Beta	SE	*p*
AK4	Direct effect	−0.0094	0.0035	0.0074	0.0206	0.0037	<0.0001	−0.0112	0.0035	0.0014
Indirect effect	through C1	−0.0032	0.0011	0.0036						
Indirect effect	through C2	−0.0019	0.0008	0.0175						
ITPK1	Direct effect	0.0075	0.0036	0.0362	0.0147	0.0038	0.0001			
Indirect effect	through C1	0.0025	0.0009	0.0077						
IGFBP5	Direct effect	−0.0142	0.0035	<0.0001	0.0185	0.0038	<0.0001	−0.0166	0.0036	<0.0001
Indirect effect	through C1	−0.0029	0.0010	0.0037						
Indirect effect	through C2	−0.0031	0.0010	0.0019						
HSPB2	Direct effect	−0.0041	0.0035	0.2479	0.0196	0.0038	<0.0001			
Indirect effect	through C1	−0.0032	0.0010	0.0014						

Cognitive decline = demographic variables + neuropathology + postmortem R_2 + protein.
Cluster group 1 was mainly located in the white matter, whereas cluster group 2 was in the gray matter.

showing higher levels of PLXNB1 contributed to increased accumulation of β-amyloid and PHFtau tangle density (Yu et al., 2018). M109, however, also has a large direct edge to cognitive decline. We found 4 proteins associated with cognitive decline that were not explained by AD and other pathologies: AK4, ITPK1, HSPB2, and IGFBP5 (Yu et al., 2018). In this study, we demonstrate that changes in the brain measured by postmortem R_2 mediate the relationship between each protein and cognitive decline. Specifically, higher abundances of AK4, HSPB2, and IGFBP5 are associated with faster cognitive decline, as mediated by postmortem R_2 clusters in extensive white matter regions, where lower R_2 is a marker of neurodegenerative/vascular disease within the white matter (Dickie et al., 2016; Fleischman et al., 2015; Gebeily et al., 2014; Williamson et al., 2018). Conversely, higher abundance of ITPK1 was associated with slower cognitive decline as mediated by postmortem R_2 clusters in the white matter, where higher white matter R_2 is a marker of tissue health. In a previous study (Yu et al., 2018), AK4 and ITPK1 abundances present a degree of resilience effect that is defined as changes in cognitive function not explained by known pathologies (Boyle et al., 2013). Of these 2 proteins, we found that ITPK1 is of particular interest, in that its higher abundance inhibits cognitive decline through increased white matter fidelity. This protective effect could be related to other factors, such as regular participation in cognitively stimulating activities, which has been shown by diffusion MRI to promote white matter microstructural integrity (Arfanakis et al., 2016). Thus, further studies on the modulating effect of ITPK1 on various risk/resilience factors in cognitive aging are warranted. If these proteins play a causal role in regulating brain structure, it may be possible to define their mechanisms of action through existing molecular studies. AK4 is a mitochondrial protein from the adenylate kinase family, whose members are involved in ubiquitous energy metabolism and homeostasis of cellular adenine nucleotide composition (Yoneda et al., 1998). A prior study found high levels of endogenous AK4 in hypoxia-treated cells and spinal cords of an ALS mouse model, suggesting enzymatically inactive AK4 is a stress responsive protein critical to cell survival and proliferation (Liu et al., 2009). HSPB2 belongs to a family of heat shock proteins, originally discovered as stress-inducible proteins and newly emerged as a regulator of physiological functions such as protein management and cell death (Stetler et al., 2010) in the central nervous system. IGFBP5 is a binding protein that regulates activity of insulin-like growth factors, which plays a crucial role in neurodevelopment and apoptosis. Evidence from mouse models show that neuronal IGFBP5 overexpression results in motor neuron degeneration and myelination defects (Marshman et al., 2003; O'Kusky and Ye, 2012; Simon et al., 2015). ITPK1 is a regulatory enzyme that plays a key role in intracellular inositol phosphate (IP) metabolism, a process that plays crucial roles in diverse cellular functions such as growth, apoptosis, migration, and differentiation. Overexpression of ITPK1 leads to increased levels of IP4 and highly phosphorylated forms of inositol in mammalian cells, including IP5 and IP6. In mice, reduced levels of ITPK1 result in the development of neural tube defects (Majerus et al., 2010; Wilson et al., 2009).

Viewing these results in light of existing literature on the function of individual proteins offers plausible mechanisms underlying the relationships among protein abundance, brain microstructure, and cognitive decline. This evidence is consistent with the directionality of our findings, namely that abundant AK4, HSPB2, and IGFBP5 are linked with faster cognitive decline via decreased brain microstructural integrity, as marked by lower R_2. In addition, hypoxia-driven demyelination is a plausible factor

Table 7
Proportion of the direct and the indirect effect to the total effect on cognition by protein

Protein	Covariates	Controlling only demographic variables		Controlling both of demographic and pathology variables	
	Effect	Effect	Proportion	Effect	Proportion
AK4	Total	−0.017	100.0%	−0.015	100.0%
	Direct	−0.009	52.9%	−0.009	60.0%
	Indirect through R_2	−0.008	47.1%	−0.006	40.0%
ITPK1	Total	0.015	100.0%	0.010	100.0%
	Direct	0.008	53.3%	0.007	70.0%
	Indirect through R_2	0.007	46.7%	0.003	30.0%
IGFBP5	Total	−0.031	100.0%	−0.020	100.0%
	Direct	−0.017	54.8%	−0.014	70.0%
	Indirect through R_2	−0.014	45.2%	−0.006	30.0%
HSPB2	Total	−0.014	100.0%	−0.007	100.0%
	Direct	−0.007	50.0%	−0.004	57.1%
	Indirect through R_2	−0.007	50.0%	−0.003	42.9%

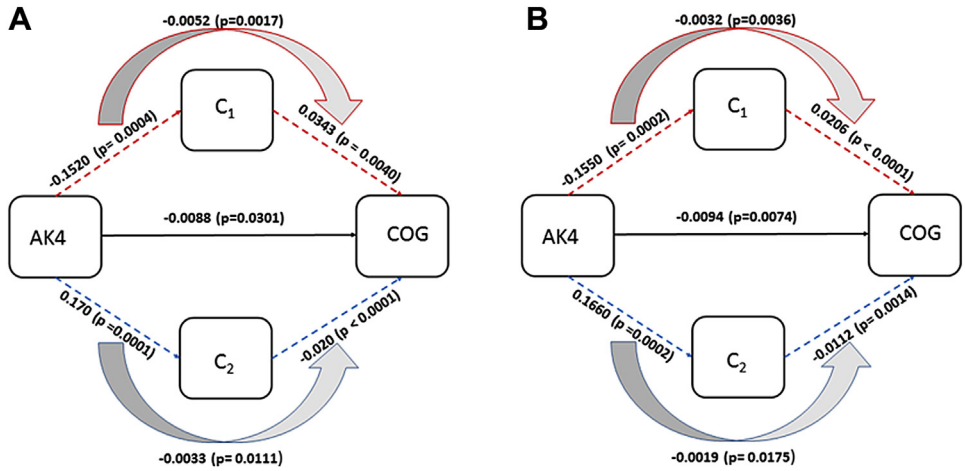

Fig. 3. Diagram for mediation of postmortem R_2 clusters (C_1, C_2) on association between AK4 and cognitive decline. (A) The effects estimated with demographic variables as covariates are shown. (B) The effects estimated with Alzheimer's disease and common neuropathology added to the covariates in (A) are shown. C_1 and C_2 are mean of the R_2 measurements from cluster groups that are associated with AK4.

underlying R_2 depression (Dawe et al., 2016). Association of ITPK1 with cognitive decline is however different from AK4, IGFBP5, and HSPB2. Namely, abundant ITPK1 seems to support rather than detract from brain tissue integrity, which would likely help to preserve cognitive abilities while manifesting as higher R_2 in extensive frontal, temporal, and parietal white matter areas. This is consistent with the fact that ITPK1 is associated with a slower rate of cognitive decline.

We hypothesized the mediation model tested in this study based on our previous study (Mostafavi et al., 2018), in which we showed that m109, a network of gene transcripts, mathematically has a causal relation with β-amyloid and a separate effect on cognitive decline independent of β-amyloid and PHFtau pathology. It was also found that manipulating some m109 genes in human astrocyte cell cultures of β-amyloid production recapitulates the predictions from the model supporting causality. The proteins of interest in this study were nominated from m109 and found to be associated with cognitive decline controlling for common brain pathologies (Yu et al., 2018). Here, we replace common brain pathologies with R_2, a proxy biomarker of microstructural changes in the brain some of which are beneficial and others deleterious. Our findings are consistent with but do not prove a causal relationship.

We examined the association of *APOE* genotype—a well-known risk factor for cognitive decline and Alzheimer's dementia—with the expression level of the 4 proteins. The mediation models were subsequently augmented with terms for *APOE ε4* genotype and APOE protein, and the results were not materially changed (data not shown).

R_2 describes the inverse of the transverse relaxation time constant, and T_2 describes the decay rate of the transverse component of magnetization. R_2 in vivo imaging is influenced by a number of factors, including the ratio of free to myelin-bound water molecules, and the presence of paramagnetic molecules, such as the iron-laden compounds ferritin and hemosiderin (Dawe et al., 2014a). Unlike in vivo imaging, natural tissue decomposition and chemical fixation cause the postmortem tissue's MRI properties to change as postmortem fixation time elapses (Dawe et al., 2009). Although we timed the vast majority of our postmortem scans to occur at a time postmortem when R_2 values throughout the brain should be relatively stable (approximately 30 days postmortem), we also conducted sensitivity analysis with postmortem fixation time elapsed as a covariate. The median postmortem fixation time elapsed was 33.7 days (mean 39.6, SD 15.1, min 22.2, max 125.9). Each step of mediation analysis was repeated with postmortem fixation time elapsed. Results were highly consistent with the results shown in Tables 1–6.

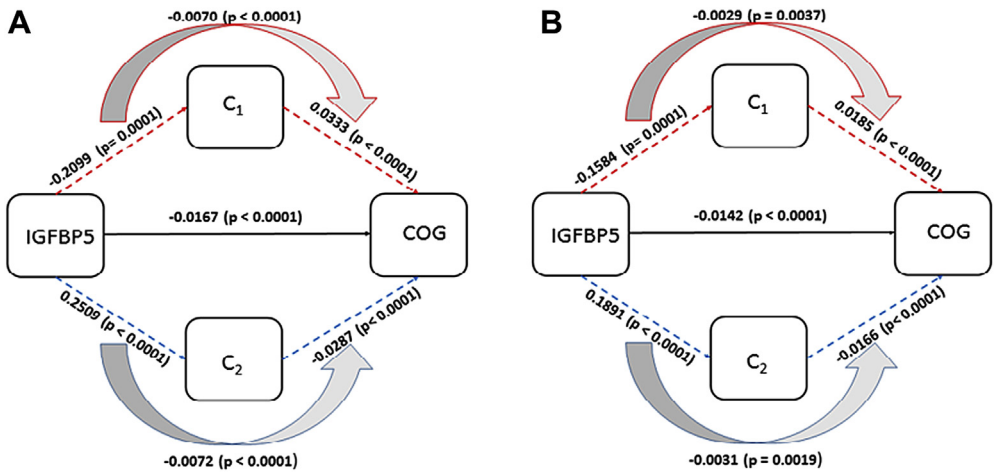

Fig. 4. Diagram for mediation of postmortem R_2 clusters (C_1, C_2) on association between IGFBP5 and cognitive decline. (A) The effects estimated with demographic variables as covariates are shown. (B) The effects estimated with Alzheimer's disease and common neuropathology added to the covariates in (A) are shown. C_1 and C_2 are mean of R_2 measurements from each cluster group that is associated with IGFBP5.

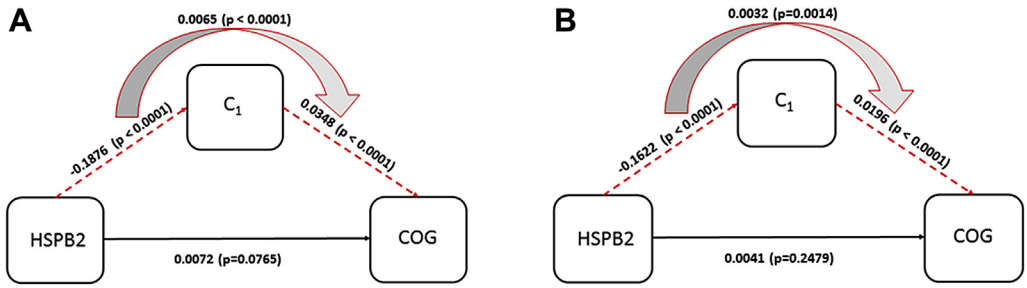

Fig. 5. Diagram for mediation of postmortem R_2 on association between HSPB2 and cognitive decline. (A) The effects estimated with demographic variables as covariates are shown. (B) The effects with AD and common neuropathology added to the covariates in (A) are shown. C_1 is mean of R_2 measurements from the cluster group that is associated with HSPB2.

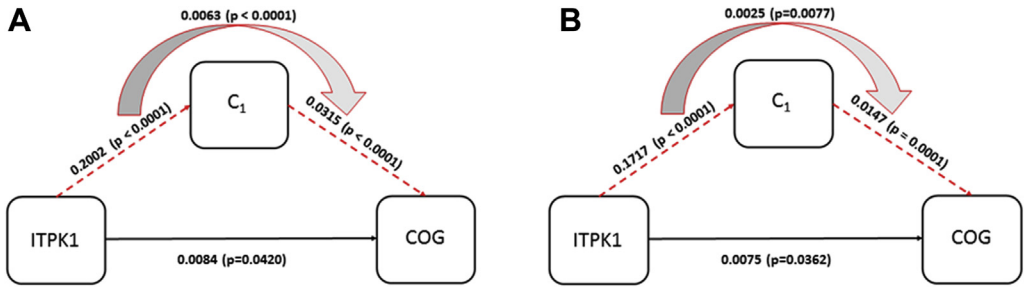

Fig. 6. Diagram for mediation of postmortem R_2 on association between ITPK1 and cognitive decline. (A) The effects estimated with demographic variables as covariates are shown. (B) The effects with AD and common neuropathology added to the covariates in (A) are shown. C_1 is mean of R_2 measurements from the cluster group that is associated with ITPK1.

Abundance of the 4 proteins from m109 in the brain were explained in part by microstructural changes in the brain measured by postmortem R_2, which accounts for a significant amount of the variance in cognitive decline. Thus, it provides a molecular anchor to an important neuroimaging feature of the aging brain. In addition, regions of the brain associated with abundances of each of the proteins overlapped extensively, which is consistent with these proteins being functionally related to one another; they were originally identified to be coexpressed at the RNA level in the same cortex, DLPFC (Mostafavi et al., 2018). We also found that the 4 proteins showed association with R_2 in areas beyond DLPFC in the postmortem brain. We previously reported R_2 associations with areas in the postmortem brain beyond the DLPFC with transcriptomic and epigenomic data as well (Gaiteri et al., 2018; Yu et al., 2017). This is expected because the DLPFC is an important hub in many functional brain networks. It is likely that such associations are best detected in normal appearing tissue in MRI but not visible lesions. Unfortunately, spatial variation in abundance of each protein across the postmortem brain is unknown and warrants further investigation.

The study has several strengths. The community-based cohort enrolls persons without dementia. The high clinical follow-up and autopsy rates result in high internal validity. Our study is based on cohorts that have relatively large sample size of longitudinal cognitive function data and the wide range of neuropathologies. However, the study also has several limitations. We select the hemisphere less affected by visible pathology for proteomics. We acknowledge that such a nonrandom selection may cause a bias in findings most likely toward the null. We also acknowledge the limitations of drawing causal inferences from cross-sectional associations. We note that, to strictly assess causal inference, it warrants further studies by manipulating those proteins in an ex vivo model system of brain microstructure. We utilized only postmortem R_2 images of which mechanism can only be attributed to increased water or iron accumulation. Further research is warranted to link these proteins to measures from antemortem imaging modalities, such as diffusion tensor imaging and resting-state functional MRI, to explain structural connection between areas in the brain and the functional connectivity.

Disclosure

The authors declare no potential conflicts of interest exist.

Acknowledgements

The authors thank all the ROS and MAP participants and also all the staff members and investigators at the Rush Alzheimer's Disease Center (RADC) for providing and processing high-quality data. In addition, the authors thank Dr Katherine Blizinsky for helpful discussions and comments. Please visit the RADC Research Resource Sharing Hub (www.radc.rush.edu) to obtain data for research purpose. This study was supported in part by NIH grants P30AG010161, R01AG15819, R01AG17917, U01AG046152, R01AG034374, 1R01AG057911, and U01AG61356.

Authors' contributions: NK, LY, RD, and DAB contributed to conception and design of the study. NK, LY, RD, VAP, JAS, and DAB contributed to acquisition and analysis of data. Drafting a significant portion of the manuscript or figures was performed by NK, LY, RD, VAP, CG, PLD, JAS, KA, and DAB.

Appendix A. Supplementary data

Supplementary data to this article can be found online at https://doi.org/10.1016/j.neurobiolaging.2019.07.013.

References

Andreev, V.P., Petyuk, V.A., Brewer, H.M., Karpievitch, Y.V., Xie, F., Clarke, J., Camp, D., Smith, R.D., Lieberman, A.P., Albin, R.L., Nawaz, Z., El Hokayem, J., Myers, A.J., 2012. Label-free quantitative LC-MS proteomics of Alzheimer's disease and normally aged human brains. J. Proteome Res. 11, 3053–3067.

Arfanakis, K., Wilson, R.S., Barth, C.M., Capuano, A.W., Vasireddi, A., Zhang, S., Fleischman, D.A., Bennett, D.A., 2016. Cognitive activity, cognitive function, and brain diffusion characteristics in old age. Brain Imaging Behav. 10, 455–463.
Arfanakis, K., Gui, M., Tamhane, A.A., Carew, J.D., 2007. Investigating the medial temporal lobe in Alzheimer's disease and mild cognitive impairment, with turboprop diffusion tensor imaging, MRI-volumetry, and T2-relaxometry. Brain Imaging Behav. 1, 11–21.
Arvanitakis, Z., Capuano, A.W., Leurgans, S.E., Buchman, A.S., Bennett, D.A., Schneider, J.A., 2017. The relationship of cerebral vessel pathology to brain microinfarcts. Brain Pathol. 27, 77–85.
Arvanitakis, Z., Leurgans, S.E., Barnes, L.L., Bennett, D.A., Schneider, J.A., 2011. Microinfarct pathology, dementia, and cognitive systems. Stroke 42, 722–727.
Arvanitakis, Z., Capuano, A.W., Leurgans, S.E., Bennett, D.A., Schneider, J.A., 2016. Relation of cerebral vessel disease to Alzheimer's disease dementia and cognitive function in elderly people: a cross-sectional study. Lancet Neurol. 15, 934–943.
Bennett, D.A., Buchman, A.S., Boyle, P.A., Barnes, L.L., Wilson, R.S., Schneider, J.A., 2018. Religious orders study and rush memory and aging project. J. Alzheimers Dis. 64, S161–S189.
Bennett, D.A., Wilson, R.S., Boyle, P.A., Buchman, A.S., Schneider, J.A., 2012. Relation of neuropathology to cognition in persons without cognitive impairment. Ann. Neurol. 72, 599–609.
Bennett, D.A., Schneider, J.A., Tang, Y., Arnold, S.E., Wilson, R.S., 2006. The effect of social networks on the relation between Alzheimer's disease pathology and level of cognitive function in old people: a longitudinal cohort study. Lancet Neurol. 5, 406–412.
Boyle, P.A., Wilson, R.S., Yu, L., Barr, A.M., Honer, W.G., Schneider, J.A., Bennett, D.A., 2013. Much of late life cognitive decline is not due to common neurodegenerative pathologies. Ann. Neurol. 74, 478–489.
Boyle, P.A., Yu, L., Nag, S., Leurgans, S., Wilson, R.S., Bennett, D.A., Schneider, J.A., 2015. Cerebral amyloid angiopathy and cognitive outcomes in community-based older persons. Neurology 85, 1930.
Dawe, R.J., Bennett, D.A., Schneider, J.A., Leurgans, S.E., Kotrotsou, A., Boyle, P.A., Arfanakis, K., 2014a. Ex vivo T2 relaxation: associations with age-related neuropathology and cognition. Neurobiol. Aging 35, 1549–1561.
Dawe, R.J., Bennett, D.A., Schneider, J.A., Vasireddi, S.K., Arfanakis, K., 2009. Postmortem MRI of human brain hemispheres: T2 relaxation times during formaldehyde fixation. Magn. Reson. Med. 61, 810–818.
Dawe, R.J., Yu, L., Leurgans, S.E., Schneider, J.A., Buchman, A.S., Arfanakis, K., Bennett, D.A., Boyle, P.A., 2016. Postmortem MRI: a novel window into the neurobiology of late life cognitive decline. Neurobiol. Aging 45, 169–177.
Dawe, R.J., Yu, L., Schneider, J.A., Arfanakis, K., Bennett, D.A., Boyle, P.A., 2018. Postmortem brain MRI is related to cognitive decline, independent of cerebral vessel disease in older adults. Neurobiol. Aging 69, 177–184.
Dickie, D.A., Ritchie, S.J., Cox, S.R., Sakka, E., Royle, N.A., Aribisala, B.S., Valdés Hernández, M.D.C., Maniega, S.M., Pattie, A., Corley, J., Starr, J.M., Bastin, M.E., Deary, I.J., Wardlaw, J.M., 2016. Vascular risk factors and progression of white matter hyperintensities in the Lothian Birth Cohort 1936. Neurobiol. Aging 42, 116–123.
Fleischman, D.A., Yang, J., Arfanakis, K., Arvanitakis, Z., Leurgans, S.E., Turner, A.D., Barnes, L.L., Bennett, D.A., Buchman, A.S., 2015. Physical activity, motor function, and white matter hyperintensity burden in healthy older adults. Neurology 84, 1294–1300.
Friston, K.J., Worsley, K.J., Frackowiak, R.S., Mazziotta, J.C., Evans, A.C., 1994. Assessing the significance of focal activations using their spatial extent. Hum. Brain Mapp. 1, 210–220.
Fulcher, B.D., Fornito, A., 2016. A transcriptional signature of hub connectivity in the mouse connectome. Proc. Natl. Acad. Sci. U. S. A. 113, 1435–1440.
Gaiteri, C., Dawe, R., Mostafavi, S., Blizinsky, K.D., Tasaki, S., Komashko, V., Yu, L., Wang, Y., Schneider, J.A., Arfanakis, K., De Jager, P.L., Bennett, D.A., 2018. Gene expression and DNA methylation are extensively coordinated with MRI-based brain microstructural characteristics. Brain Imaging Behav. 13, 963–972.
Gebeily, S., Fares, Y., Kordahi, M., Khodeir, P., Labaki, G., Fazekas, F., 2014. Cerebral white matter hyperintensities (WMH): an analysis of cerebrovascular risk factors in Lebanon. Int. J. Neurosci. 124, 799–805.
Hayes, A.F., Preacher, K.J., 2014. Statistical mediation analysis with a multicategorical independent variable. Br. J. Math. Stat. Psychol. 67, 451–470.
House, M.J., St Pierre, T.G., Foster, J.K., Martins, R.N., Clarnette, R., 2006. Quantitative MR imaging R2 relaxometry in elderly participants reporting memory loss. AJNR Am. J. Neuroradiol. 27, 430–439.
House, M.J., St Pierre, T.G., McLean, C., 2008. 1.4T study of proton magnetic relaxation rates, iron concentrations, and plaque burden in Alzheimer's disease and control postmortem brain tissue. Magn. Reson. Med. 60, 41–52.
Kim, M., Pinto, S.M., Getnet, D., Nirujogi, R.S., Manda, S.S., Chaerkady, R., Madugundu, A.K., Kelkar, D.S., Isserlin, R., Jain, S., Thomas, J.K., Muthusamy, B., Leal-Rojas, P., Kumar, P., Sahasrabuddhe, N.A., Balakrishnan, L., Advani, J., George, B., Renuse, S., Selvan, L.D.N., Patil, A.H., Nanjappa, V., Radhakrishnan, A., Prasad, S., Subbannayya, T., Raju, R., Kumar, M., Sreenivasamurthy, S.K., Marimuthu, A., Sathe, G.J., Chavan, S., Datta, K.K., Subbannayya, Y., Sahu, A., Yelamanchi, S.D., Jayaram, S., Rajagopalan, P., Sharma, J., Murthy, K.R., Syed, N., Goel, R., Khan, A.A., Ahmad, S., Dey, G., Mudgal, K., Chatterjee, A., Huang, T., Zhong, J., Wu, X., Shaw, P.G., Freed, D., Zahari, M.S., Mukherjee, K.K., Shankar, S., Mahadevan, A., Lam, H., Mitchell, C.J., Shankar, S.K., Satishchandra, P., Schroeder, J.T., Sirdeshmukh, R., Maitra, A., Leach, S.D., Drake, C.G., Halushka, M.K., Prasad, T.S.K., Hruban, R.H., Kerr, C.L., Bader, G.D., Iacobuzio-Donahue, C., Gowda, H., Pandey, A., 2014. A draft map of the human proteome. Nature 509, 575.
Kirsch, S.J., Jacobs, R.W., Butcher, L.L., Beatty, J., 1992. Prolongation of magnetic resonance T2 time in hippocampus of human patients marks the presence and severity of Alzheimer's disease. Neurosci. Lett. 134, 187–190.
Krienen, F.M., Yeo, B.T., Ge, T., Buckner, R.L., Sherwood, C.C., 2016. Transcriptional profiles of supragranular-enriched genes associate with corticocortical network architecture in the human brain. Proc. Natl. Acad. Sci. U. S. A. 113, E469–E478.
Liu, R., Strom, A.L., Zhai, J., Gal, J., Bao, S., Gong, W., Zhu, H., 2009. Enzymatically inactive adenylate kinase 4 interacts with mitochondrial ADP/ATP translocase. Int. J. Biochem. Cell Biol. 41, 1371–1380.
Majerus, P.W., Wilson, D.B., Zhang, C., Nicholas, P.J., Wilson, M.P., 2010. Expression of inositol 1,3,4-trisphosphate 5/6-kinase (ITPK1) and its role in neural tube defects. Adv. Enzyme Regul. 50, 365–372.
Marshman, E., Green, K.A., Flint, D.J., White, A., Streuli, C.H., Westwood, M., 2003. Insulin-like growth factor binding protein 5 and apoptosis in mammary epithelial cells. J. Cell. Sci. 116, 675.
Mostafavi, S., Gaiteri, C., Sullivan, S.E., White, C.C., Tasaki, S., Xu, J., Taga, M., Klein, H.U., Patrick, E., Komashko, V., McCabe, C., Smith, R., Bradshaw, E.M., Root, D.E., Regev, A., Yu, L., Chibnik, L.B., Schneider, J.A., Young-Pearse, T.L., Bennett, D.A., De Jager, P.L., 2018. A molecular network of the aging human brain provides insights into the pathology and cognitive decline of Alzheimer's disease. Nat. Neurosci. 21, 811–819.
Nag, S., Yu, L., Capuano, A.W., Wilson, R.S., Leurgans, S.E., Bennett, D.A., Schneider, J.A., 2015. Hippocampal sclerosis and TDP-43 pathology in aging and Alzheimer disease. Ann. Neurol. 77, 942–952.
O'Kusky, J., Ye, P., 2012. Neurodevelopmental effects of insulin-like growth factor signaling. Front. Neuroendocrinol. 33, 230–251.
Petyuk, V.A., Qian, W.J., Smith, R.D., Smith, D.J., 2010. Mapping protein abundance patterns in the brain using voxelation combined with liquid chromatography and mass spectrometry. Methods 50, 77–84.
Richiardi, J., Altmann, A., Milazzo, A.C., Chang, C., Chakravarty, M.M., Banaschewski, T., Barker, G.J., Bokde, A.L., Bromberg, U., Buchel, C., Conrod, P., Fauth-Buhler, M., Flor, H., Frouin, V., Gallinat, J., Garavan, H., Gowland, P., Heinz, A., Lemaitre, H., Mann, K.F., Martinot, J.L., Nees, F., Paus, T., Pausova, Z., Rietschel, M., Robbins, T.W., Smolka, M.N., Spanagel, R., Strohle, A., Schumann, G., Hawrylycz, M., Poline, J.B., Greicius, M.D., 2015. IMAGEN consortium, 2015. BRAIN NETWORKS. Correlated gene expression supports synchronous activity in brain networks. Science 348, 1241–1244.
Schneider, J.A., Arvanitakis, Z., Leurgans, S.E., Bennett, D.A., 2009. The neuropathology of probable Alzheimer disease and mild cognitive impairment. Ann. Neurol. 66, 200–208.
Schneider, J.A., Arvanitakis, Z., Yu, L., Boyle, P.A., Leurgans, S.E., Bennett, D.A., 2012. Cognitive impairment, decline and fluctuations in older community-dwelling subjects with Lewy bodies. Brain 135, 3005–3014.
Simon, C.M., Rauskolb, S., Gunnersen, J.M., Holtmann, B., Drepper, C., Dombert, B., Braga, M., Wiese, S., Jablonka, S., Pühringer, D., Zielasek, J., Hoeflich, A., Silani, V., Wolf, E., Kneitz, S., Sommer, C., Toyka, K.V., Sendtner, M., 2015. Dysregulated IGFBP5 expression causes axon degeneration and motoneuron loss in diabetic neuropathy. Acta Neuropathol. 130, 373–387.
Stetler, R.A., Gan, Y., Zhang, W., Liou, A.K., Gao, Y., Cao, G., Chen, J., 2010. Heat shock proteins: cellular and molecular mechanisms in the central nervous system. Prog. Neurobiol. 92, 184–211.
Wang, H., Yuan, H., Shu, L., Xie, J., Zhang, D., 2004. Prolongation of T(2) relaxation times of hippocampus and amygdala in Alzheimer's disease. Neurosci. Lett. 363, 150–153.
Williamson, W., Lewandowski, A.J., Forkert, N.D., al, e., 2018. Association of cardiovascular risk factors with MRI indices of cerebrovascular structure and function and white matter hyperintensities in young adults. JAMA 320, 665–673.
Wilson, M.P., Hugge, C., Bielinska, M., Nicholas, P., Majerus, P.W., Wilson, D.B., 2009. Neural tube defects in mice with reduced levels of inositol 1,3,4-trisphosphate 5/6-kinase. Proc. Natl. Acad. Sci. U. S. A. 106, 9831–9835.
Worsley, K.J., Marrett, S., Neelin, P., Vandal, A.C., Friston, K.J., Evans, A.C., 1996. A unified statistical approach for determining significant signals in images of cerebral activation. Hum. Brain Mapp. 4, 58–73.
Yoneda, T., Sato, M., Maeda, M., Takagi, H., 1998. Identification of a novel adenylate kinase system in the brain: cloning of the fourth adenylate kinase. Brain Res. Mol. Brain Res. 62, 187–195.
Yu, L., Boyle, P.A., Nag, S., Leurgans, S., Buchman, A.S., Wilson, R.S., Arvanitakis, Z., Farfel, J.M., De Jager, P.L., Bennett, D.A., Schneider, J.A., 2015a. APOE and cerebral amyloid angiopathy in community-dwelling older persons. Neurobiol. Aging 36, 2946–2953.
Yu, L., Dawe, R.J., Boyle, P.A., Gaiteri, C., Yang, J., Buchman, A.S., Schneider, J.A., Arfanakis, K., De Jager, P.L., Bennett, D.A., 2017. Association between brain gene expression, DNA methylation, and alteration of ex vivo magnetic resonance imaging transverse relaxation in late-life cognitive decline. JAMA Neurol. 74, 1473–1480.
Yu, L., De Jager, P.L., Yang, J., Trojanowski, J.Q., Bennett, D.A., Schneider, J.A., 2015b. The TMEM106B locus and TDP-43 pathology in older persons without FTLD. Neurology 84, 927–934.
Yu, L., Petyuk, V.A., Gaiteri, C., Mostafavi, S., Young-Pearse, T., Shah, R.C., Buchman, A.S., Schneider, J.A., Piehowski, P.D., Sontag, R.L., Fillmore, T.L., Shi, T., Smith, R.D., De Jager, P.L., Bennett, D.A., 2018. Targeted brain proteomics uncover multiple pathways to Alzheimer's dementia. Ann. Neurol. 84, 78–88.